Hindawi Publishing Corporation
Journal of Nanotechnology
Volume 2016, Article ID 5135420, 9 pages
http://dx.doi.org/10.1155/2016/5135420

Research Article

Synthesis of Graphene-Based Nanocomposite and Investigations of Its Thermal and Electrical Properties

Manoj Kumar Pati,[1] Puspalata Pattojoshi,[1] and Gouri Sankar Roy[2]

[1]*Department of Physics, KIIT University, Bhubaneswar, Odisha 751024, India*
[2]*PG Department of Physics, College of Engineering and Technology, Bhubaneswar, Odisha 751003, India*

Correspondence should be addressed to Manoj Kumar Pati; manojkumarpati43@gmail.com

Received 15 April 2016; Revised 21 June 2016; Accepted 22 June 2016

Academic Editor: Simon Joseph Antony

We describe the synthesis of acid functionalized graphene (GE) which is grafted to chitosan (CH) by first reacting the oxidized GE with thionyl chloride to form acyl-chlorinated GE. This product is subsequently dispersed in chitosan and covalently grafted to form GE-chitosan. GE-chitosan is further grafted onto polymetanitroaniline (PMNA) by free radical polymerization conditions to yield GE-CH-PMNA. We have characterized the structure of synthesized GE-CH-PMNA composites by X-ray diffraction (XRD), Fourier transform infrared spectroscopy (FTIR), thermogravimetric analysis (TGA), scanning electron microscopy, and conductivity measurements. XRD data suggest the strongly crystalline character of the prepared specimen. Our measurement shows that the dielectric constants of these nanocomposites are remarkably enhanced due to interfacial polarization effect. This study demonstrates that functionalized graphene sheets are ideal nanofillers for the development of new polymer composites with high dielectric constant values.

1. Introduction

Graphene is the most basic form of carbon. It is composed of sp^2 bonded carbon atoms arranged in a hexagonal arrangement in a 2D plane [1]. The lattice of graphene consists of two interleaved triangular shaped carbon sublattices. The sublattices overlap in such a way that carbon atom from one sublattice is at the centroid of the other sublattice [2–4]. Graphene has been used in many engineering and industrial applications to create composite materials with superior qualities such as lubricants, functional fluids, and high temperature gaskets. In these applications, one-carbon-atom thick graphene can be a very promising reinforcing agent [5–7] and provide exceptional electrical and thermal transport properties compared to other nanomaterials such as layered silicates or CNTs [8–10]. Graphene-based polymer nanocomposites exhibit superior properties of graphene [11]. For example, graphene-based polymer composites show better mechanical, thermal, and electrical properties than the neat polymer [12]. It has been shown that the mechanical and electrical properties of graphene-based polymer composites are much better in comparison to clay or other carbon filler-based polymer composites [13–17].

Due to high electrical conductivity, chemically modified graphene composites have been studied for potential electronic device applications such as photovoltaic solar cells and field effect transistors [18]. Similarly, graphene composites incorporating conductive polymers have also been studied for energy storage [19]. Besides being used in devices, polymer based graphene nanocomposites are also envisioned for a wide range of chemical and biochemical sensing applications [20]. Physical and chemical properties of the graphene-based polymer nanocomposite depend on the distribution of graphene layers in the polymer matrix and the interfacial bonding between the graphene layers and polymer matrix. However, pristine graphene does not form homogeneous composites, since it is not compatible with organic polymers. On the other hand, graphene oxide (GO) sheets which are heavily oxygenated graphene are compatible with organic polymers [21–26]. Therefore, GO is widely used as nanofiller for polymer nanocomposites. Unlike graphene, GO is

electrically insulating and therefore cannot be used for synthesizing conducting nanocomposites.

Chitosan (CH) is a naturally semicrystalline cationic polysaccharide, which has found widespread applications as a biopolymer in tissue engineering and drug delivery applications [27]. Chitosan forms composites with GO sheets. The positive value of zeta potential of CH is caused by protonated amino groups while the negative zeta potential for GO suspension is caused by deprotonated carboxyl groups [28–30]. The effect of GO on the properties of CH films has been studied by Han et al. [31] by preparing CH/GO nanocomposites using solution mixing method. Strong interactions between the functional groups of the two components have been observed, which led to improved mechanical strength in both wet and dry state, storage modulus, and thermal stability for the CH/GO nanocomposite. Similar mechanical and thermal properties have also been observed in CH/Reduced GO (RGO) nanocomposites by Wang et al. [32]. Tensile strength of this CH/RGO nanocomposite was measured to be higher than that of pure chitosan, while it also exhibited high electrical conductivity. Graphene/CH nanocomposites have also been developed for electrochemical sensor applications for which properties such as high electrical conductivity and electron transfer rate of graphene are highly suitable [33]. In this study, the redox peak current of 4-aminophenol was found to be enhanced indicating the electrocatalytic effect of graphene.

GO/CH nanocomposite films containing chitosan were recently prepared via solution mixing (i.e., sonochemical method) for use in electrochemical biosensors [34]. Presence of GO revealed improved thermal stability, increased glass transition temperature, and storage modulus of the GO/CH nanocomposite film. Cyclic voltammetric experiment showed that the GO/CH modified electrode exhibited higher electrocatalytic activity than neat CH. The GO/CH composite suspension yields a suspension with a zeta potential of ~51 mV due to strong ionic interactions between positively charged CH and negatively charged GO. It is important to note that this suspension with zeta potential higher than 30 mV is considered to be stable [35]. Homogeneous GO/CH suspensions are prepared by adding GO to the solution of chitosan [36]. The GO/CH composite film is formed by electrodeposition on the surface of the cathode [37].

In this paper, we discuss the synthesis of a particular type of graphene-based nanocomposite using CH and polymetanitroaniline (PMNA) and investigate its physical, chemical, and electrical properties with different compositions. PMNA is a conducting polymer widely used in the fabrication of electrodes and sensors. The novelty of our research lies in synthesizing functionalized graphene attached with the natural polymer chitosan and then cross-linking with PMNA to produce a new type of graphene/conducting polymer composite. Chemical modifications of GE-CH-PMNA nanocomposite are confirmed using a number of material characterization techniques such as X-ray diffraction (XRD), scanning electron microscope (SEM), and Fourier transform infrared spectroscopy (FTIR). Physical and electrical properties such as material decomposition, heat capacity, dielectric constant, and conductivity of the GE-CH-PMNA nanocomposite are determined from thermogravimetric analysis (TGA), differential scanning colorimetry (DSC), and electronic measurements. In this research, we have demonstrated that the combination of graphene and the conducting polymer PMNA leads to a synergistic composite material possessing the properties of each of the constituent components. The dielectric constant of this composite is increased with the increase in the volume fraction of functionalized GE (F-GE) and reaches a maximum value of 3200 at 8 vol% of F-GE.

2. Materials and Methods

2.1. Materials. Graphene (GE), chitosan (CH), and PMNA used in our studies were purchased from Sigma-Aldrich. Analytical grade chemical reagents like potassium persulfate ($K_2S_2O_8$) and hydrochloric, sulfuric, and nitric acid used in our experiments were obtained from Sigma Chemicals. Figure 1 illustrates the basic reaction scheme used in the synthesis of GE-CH-PMNA nanocomposite. In the following section, we first describe the process used to prepare functionalized graphene. Next, we describe how we took advantage of the existence of some of the free amino groups in chitosan to graft functionalized graphene with chitosan and further with PMNA to produce GE-CH-PMNA nanocomposites.

2.2. Synthesis of Functionalized Graphene. Functionalized graphene was synthesized as described in our previous work [38]. Typically, GE was reacted with H_2SO_4 and HNO_3 acids with 3 : 1 ratio and later sonicated for 30 minutes using an ultrasonic sonicator to form carboxylic acid functionalized GE (GE-COOH). The carboxylic acid group was converted to formyl chloride by reaction with thionyl chloride for 24 h at 75°C. This resulted in functionalized GE-COCl as shown by the reaction scheme in Figure 1. The reaction was stopped, and the mixture was cooled before centrifuging and washing to remove excess reactants. The sample was then dried overnight at a temperature of 90°C and 30 Hg pressure.

2.3. Synthesis of GE-Chitosan. As shown by the reaction scheme in Figure 1, the functionalized GE-COCl (400 mg) was further reacted with chitosan (2 g) in 100 mL 2% acetic acid at 75°C for 24 hours while stirring. This resulted in GE-chitosan. For removing the unreacted chitosan, the product was washed three times with 2% acetic acid after the reaction was stopped.

2.4. Synthesis of GE-Chitosan Grafted Derivative. GE-chitosan (0.1 g) was again reacted with $K_2S_2O_8$ (0.02 g) and PMNA (8 mL) in 2% acetic acid solution at 75°C for 2 h to form the nanocomposite product GE-CH-PMNA. The final product was prepared by centrifuging at 20,000 rpm and washing the sample twice with water before drying at 90°C.

3. Results and Discussions

The structural, thermal, and electrical measurements were carried out on GE-CH-PMNA composite, and the important and interesting results obtained from the above characterization techniques are described below sequentially.

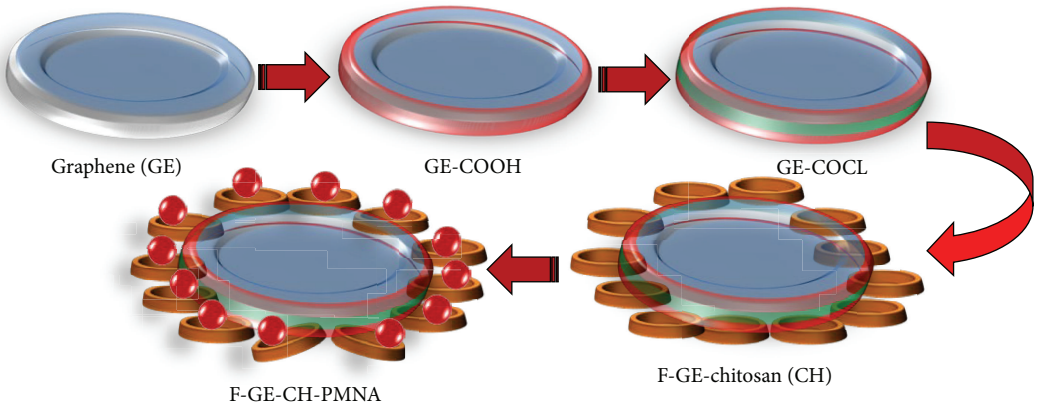

Figure 1: Reaction scheme used in the synthesis of GE-CH-PMNA.

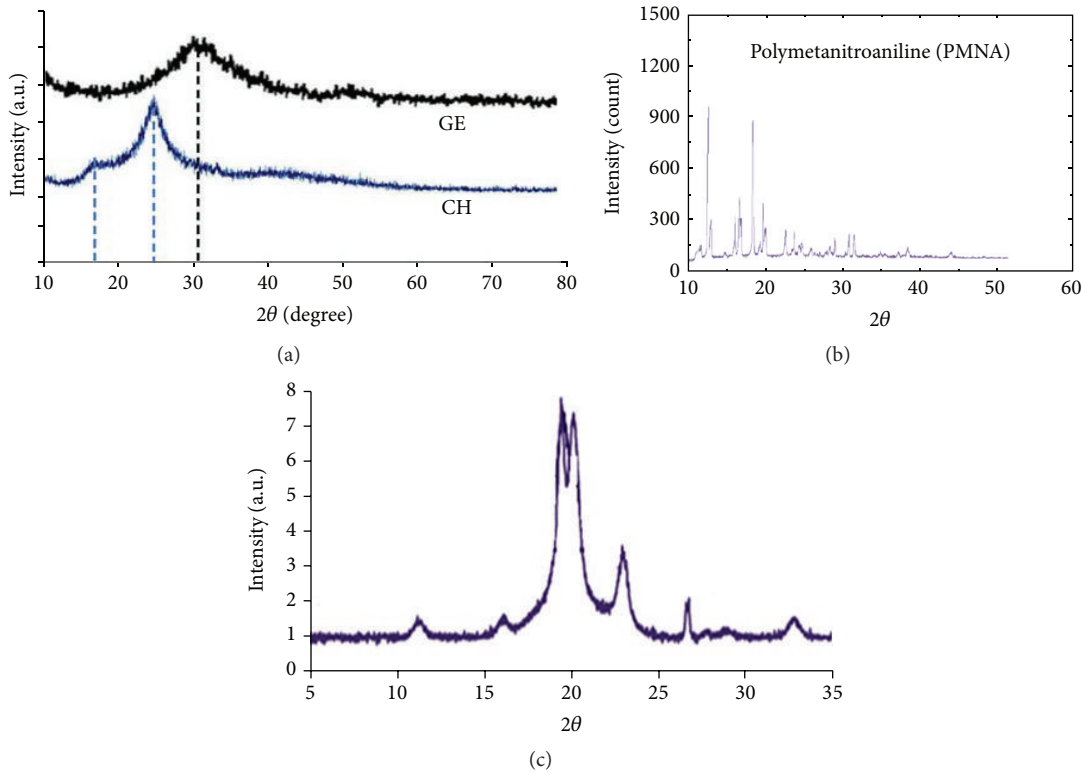

Figure 2: XRD measurements of (a) GE and CH, (b) PMNA, and (c) GE-CH-PMNA composite.

3.1. XRD Measurements. X-ray diffraction (Rigaku, D/Max, 2500 V, Cu-Kα radiation: 1.54056 Å) experiments were carried out on graphene, chitosan, and the composite GE-CH-PMNA sample. Wide-angle X-ray diffractograms were recorded in the range of 0–80° (2θ) angle keeping the sample at temperature 30°C. In Figure 2(a), the XRD pattern of chitosan shows broad diffraction peaks at 18° and 25° which are the typical fingerprints of semicrystalline chitosan. Graphene shows a strong and sharp peak at 32° indicating a higher ordered structure. Figure 2(b) shows the recorded XRD spectrum of PMNA with diffraction peaks appearing at 12.3°, 16.9°, 18.8°, and 22.6°. Using these peaks as spectral signatures, we can determine the presence of PMNA and its crystal state in the composite. Figure 2(c) shows the XRD pattern of the composite GE-CH-PMNA producing multiple peaks corresponding to 2θ at 19°, 21.9°, 23°, 27°, and 34° due to the presence of CH-PMNA along with GE. The XRD pattern of the GE-CH-PMNA composite contains all peaks assigned to both GE and the individual matrix, and it also shows sharp new peaks formed due to increase in ordering of the polymer composite. This indicates that the crystalline structure of GE is strongly influenced by the addition of CH-PMNA. The

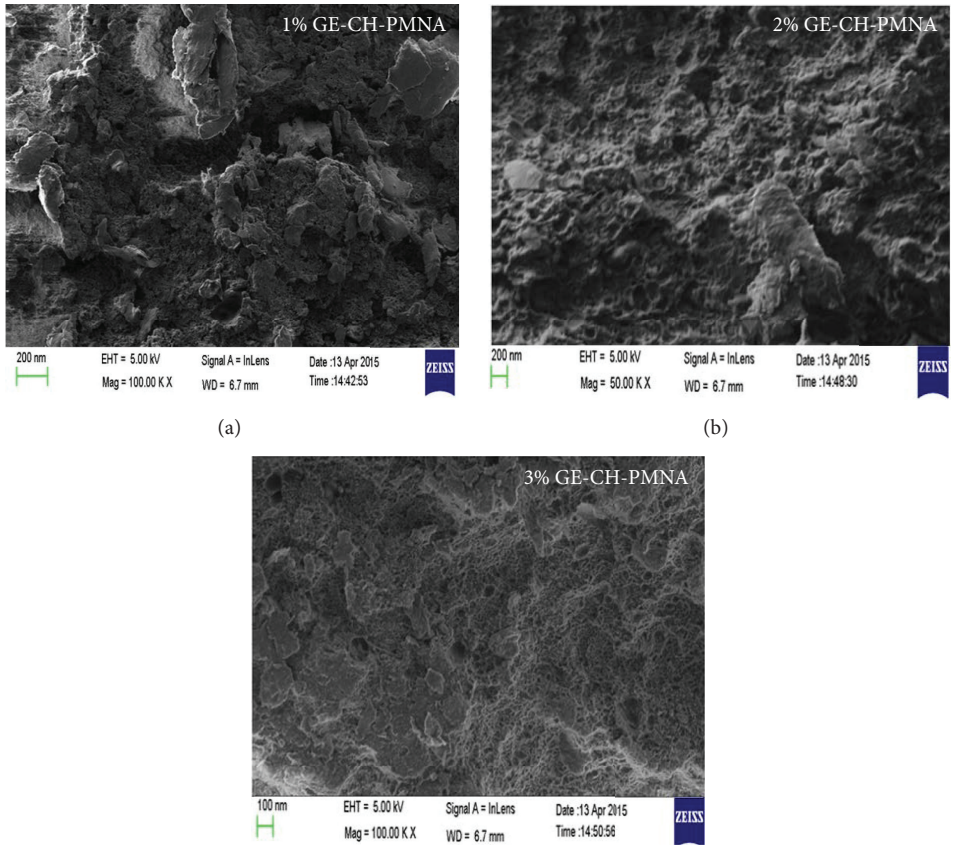

Figure 3: SEM images showing cross sections of GE-CH-PMNA composites with 1 wt%, 2 wt%, and 3 wt% of CH, respectively.

XRD result also shows that GE has been efficiently exfoliated within the CH matrix due to the presence of diminished peak at 32°.

3.2. Characterization Using SEM Image. The surface morphology of the GE-CH-PMNA nanocomposite was investigated by a scanning electron microscope (SEM, Zeiss). In order to investigate the influence of the graphene chemical functionalities on the morphology of graphene-based composites, GE and copolymer-modified graphene were blended with the polymer matrix. The SEM images in Figure 3 show the cross sections of composites containing 1 wt%, 2 wt%, and 3 wt% of CH in GE-CH-PMNA. The images show GE-PMNA is dispersed in the composite due to the formation of agglomerates at length scales of tens of microns. Figures 3(b) and 3(c) show a better distribution of GE particles homogeneously covered by the polymer. The copolymer-modified graphene composite can be homogeneously integrated within hydrophilic CH matrix. The presence of ionic moieties such as alkyl amino- and carboxylates in the polymer backbone can result in enhanced interfacial interactions between the filler and the matrix.

3.3. FTIR Spectra. The Fourier transform infrared (FTIR) spectra for various samples have been obtained using a Nicolet 8700 spectrometer, in the range of 500–4,000 cm^{-1}. Figure 4(a) shows the FTIR spectra of neat chitosan and graphene along with functionalized graphene (F-GE). The FTIR spectrum of chitosan shows a broad absorption band between 3500 cm^{-1} and 2500 cm^{-1}, centered at 3200 cm^{-1}, due to O–H stretching vibration, N–H extension vibration, and the intermolecular H-bonds of the polysaccharide moieties. A spectral band at 2790 cm^{-1} is observed which corresponds to the axial stretching of C–H bonds. A peak at 1673 cm^{-1} is observed which corresponds to the axial stretching of C=O bonds of the acetamide group. Another spectral band at 1559 cm^{-1} is observed which is related to the angular deformation of N–H bonds of the amino group. A band at 1372 cm^{-1} due to symmetrical angular deformation of CH_3 and the amide III band at 1322 cm^{-1} are also observed. Spectral band corresponding to the polysaccharide skeleton, including vibrations of the glycoside bonds, and C–O and C–O–C stretching in the range 1156–800 cm^{-1} are also observed [39, 40] in the FTIR spectrum of chitosan. Similarly, the FTIR peak of GE in Figure 4(a) shows prominent O–H stretching vibrations observed at 3453 cm^{-1}. Stretching vibrations from C=O are observed at 1735 cm^{-1} whereas the C–O stretching vibrations at 1660 cm^{-1} are also observed. In case of F-GE, multiple FTIR peaks at 3447 cm^{-1} (–OH stretching),

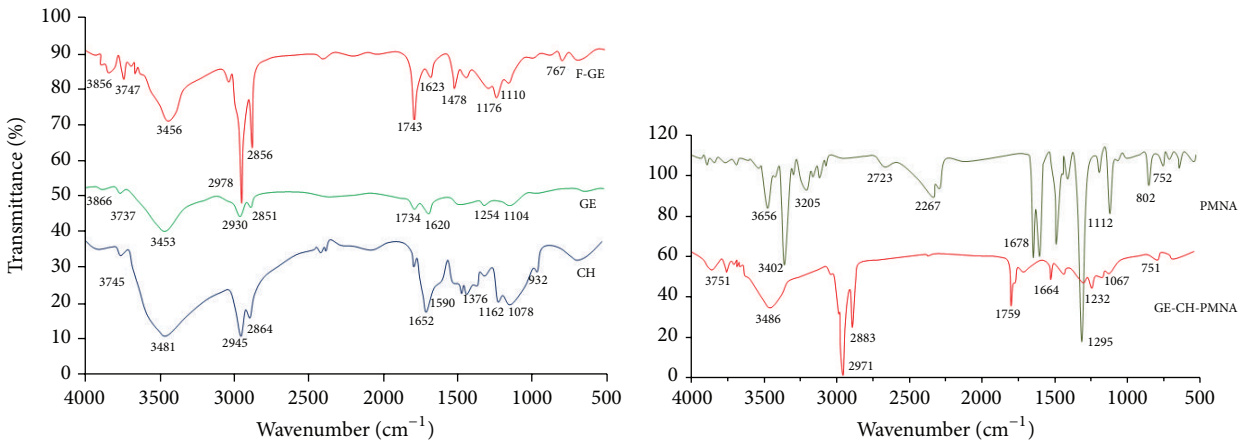

FIGURE 4: FTIR spectra obtained for (a) CH, GE, and functionalized GE (F-GE) and compared with those for (b) PMNA and GE-CH-PMNA composite.

2894 cm^{-1} (–O–H stretch), 1692 cm^{-1} (C=C ring stretching), 1385 cm^{-1} [υ(C=C), δ(O–H), υ(C–O)], 1110 cm^{-1} (C–O stretch), 891 cm^{-1} (alkyl halide stretch), and 651 cm^{-1} (C–Cl stretch) are observed which are formed by the functional carboxyl group.

Figure 4(b) shows the FTIR spectra of PMNA used in cross-linking and the GE-CH-PMNA nanocomposite. The FTIR spectrum of PMNA shows the vibration modes of benzene and quinoid rings appearing at 1513 cm^{-1}. The presence of bands in FTIR spectrum in the region extending from 741 cm^{-1} confirms that there are 1,2,4-tri-substituted rings in the polymeric backbones. The FTIR spectrum of the electrodeposited GE-CH-PMNA film showed bands at 1585 and 1410 cm^{-1}, which may be assigned to typical PMNA ring vibrations. The spectral band at 1245 cm^{-1} corresponds to –C–H bond in-plane vibrations. The peak at 1175 cm^{-1} is assigned to the N–C stretching vibration, and the band at 1098 cm^{-1} verified the presence of polymerized polymetanitroaniline. The FTIR peak observed at 3434 cm^{-1} is attributed to hydroxyl stretching vibrations of –C–OH in graphene. Table 1 provides the dip positions and their origin in the FTIR spectra shown in Figure 4(b) for PMNA and the prepared GE-CH-PMNA nanocomposite sample.

3.4. TGA Measurements. Thermogravimetric analysis (TGA) of the composite material has been carried out using TGA instrument TGA/SDTA851 at 20 μC/min heating rate under nitrogen. The thermal stability of the composite material has been assessed by TGA while keeping the material in an inert atmosphere. Figure 5(a) shows the onset temperature for pure CH degradation at about 350°C, which is attributed to the main-chain pyrolysis. At about 450°C, the total amount of polymer seemed to be pyrolyzed. It is found from Figure 5(a) that the samples containing 1 wt% GE and 1% GE-CH exhibited similar thermal stability. This can be explained by the following. The initial weight loss due to evaporation of solvent occurs at low temperature which is common to both pure GE and GE-CH. With the increase of temperature beyond 300°C, typically weight loss due to the change of mode (or phase) occurs in the sample. The identical thermal behavior of the pure GE and GE-CH probably indicates that CH remains inert in case of GE-CH composite. Figure 5(b)

TABLE 1: FTIR dip positions and their origin for PMNA and GE-CH-PMNA.

Chemical	Peak position (cm^{-1})	Assignment
PMNA	3656	OH stretching
	3402	OH stretching
	3205	–O–H stretch
	2723	C–H medium
	2267	Alkynes stretch
	1678	Alkenes stretch
	1513	Benzene and quinoid ring
	1295	Amine stretch
	1112	C–N medium
	802	Alkyl halide stretch
	741	C–Cl stretch
GE-CH-PMNA	3751	–OH stretching
	3434	–OH stretching
	2971	–O–H stretch
	2883	$-CH_2$
	1775	C=O stretching arising from carbonyl and carboxylic groups
	1664	C=N medium
	1585	PMNA ring vibration
	1410	PMNA ring vibration
	1245	C–O strong
	1175	N–C stretching
	1098	C–O stretch
	751	=C–H bending

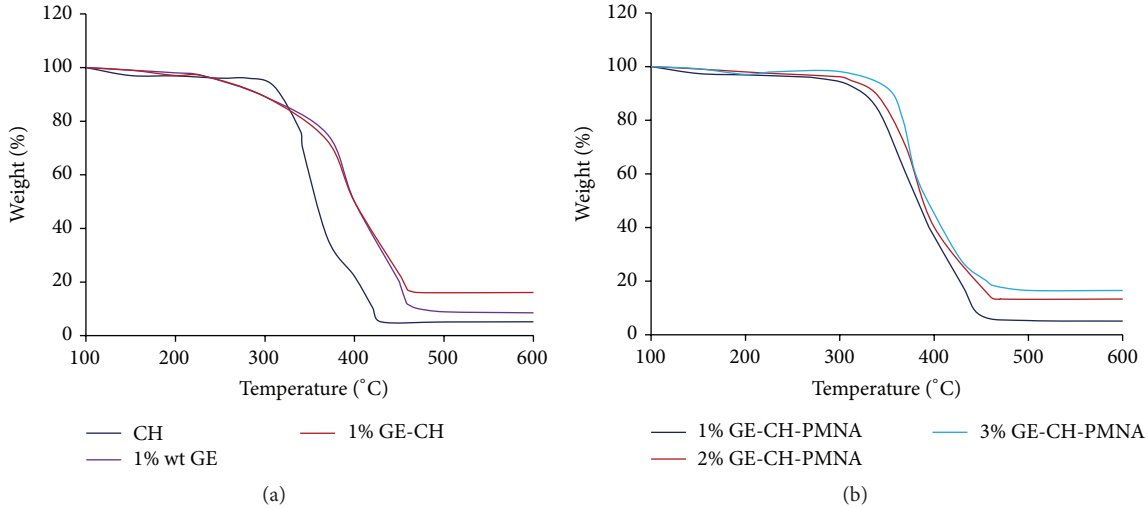

Figure 5: TGA profiles for (a) CH, 1 wt% GE, and 1% GE-CH and (b) 1, 2, and 3 wt% GE-CH-PMNA.

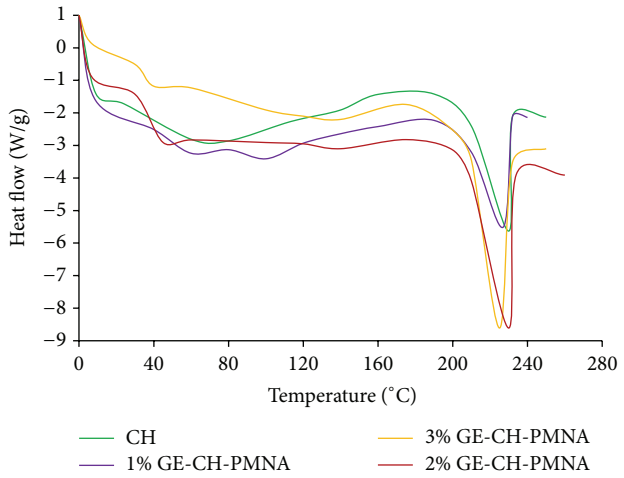

Figure 6: DSC thermograms of CH, 1% GE-CH-PMNA, 2% GE-CH-PMNA, and 3% GE-CH-PMNA.

shows TGA profiles for 1, 2, and 3 wt% GE-based composites. These materials also exhibit similar thermal stability except the fact that 1 wt% GE-based composite shows higher weight loss compared to others at the same temperature. The initial degradation observed between 200 and 280°C in these composites is attributed to the elimination of the oxygen-containing groups in the oxidized graphene nanoplatelets. The second degradation observed between 350 and 480°C happens due to the degradation of the polymer itself [34]. These results also suggest that there is a strong interaction between CH and GE nanoplatelets at the interface, and the mobility of the polymer chains near the interface is decreased because of this interaction.

3.5. DSC Measurements. Differential scanning calorimetry (DSC) measurements have been carried out to confirm strong interaction of the prepared graphene nanostructures with the polymer matrix. DSC thermograms shown in Figure 6 are obtained for CH, 1% GE-CH-PMNA, and GE-CH-PMNA composites with 2 and 3 wt%. From these heat scans, one can see the integrated area of the melting transition (ΔHm) of the samples, containing copolymer-modified GE composite. In this GE weight fraction, it is estimated that the relative crystallinity of the copolymer-modified GE/CH sample has been increased by about 5%, compared to the one of neat matrix. This crystallinity increase indicates that the polymer chains were indeed immobilized by hydrophobic and/or hydrogen bonding interactions with the GE. Overall, the order of relative crystallinity in our samples (at 1 wt% graphene loading) for copolymer-modified GE is found to be greater than the neat matrix. The fact that the sample of 3% wt GE exhibited a 15% decrease in crystallinity compared to neat CH could be attributed to the inhomogeneous dispersion of GE aggregates into the matrix. The melting endothermic peak of neat matrix (at about 230°C) was slightly decreased in the composites. This could be attributed to the relatively smaller crystal size of CH due to the intercalation of GE [41].

3.6. Dielectric and Conductivity Properties of GE-CH-PMNA. Figure 7(a) shows the electrical conductivity and the dielectric constants of the GE-CH-PMNA composites as a function of the volume fraction of the functionalized GE (F-GE) measured at room temperature and 1 kHz. The electrical conductivity of the composite is increased by more than five orders of magnitude with increase in F-GE concentration. The conductivity for the composite material can be analyzed by the following scaling equation [41, 42]:

$$\sigma_{\text{eff}} = \sigma_i \left(p_{\text{GE}} - p_c\right)^t, \quad (1)$$

where σ_i is related to bulk electrical conductivity of GE, p_{GE} is the weight fraction of F-GE, p_c is the percolation threshold, and t is the critical exponent. The conductivity of GE-CH-PMNA composite increases near the percolation threshold p_c which is found to be 3.5 vol%. Beyond the threshold, it exhibits a typical insulator-conductor transition. Conductivity of GE-CH-PMNA composites below the percolation

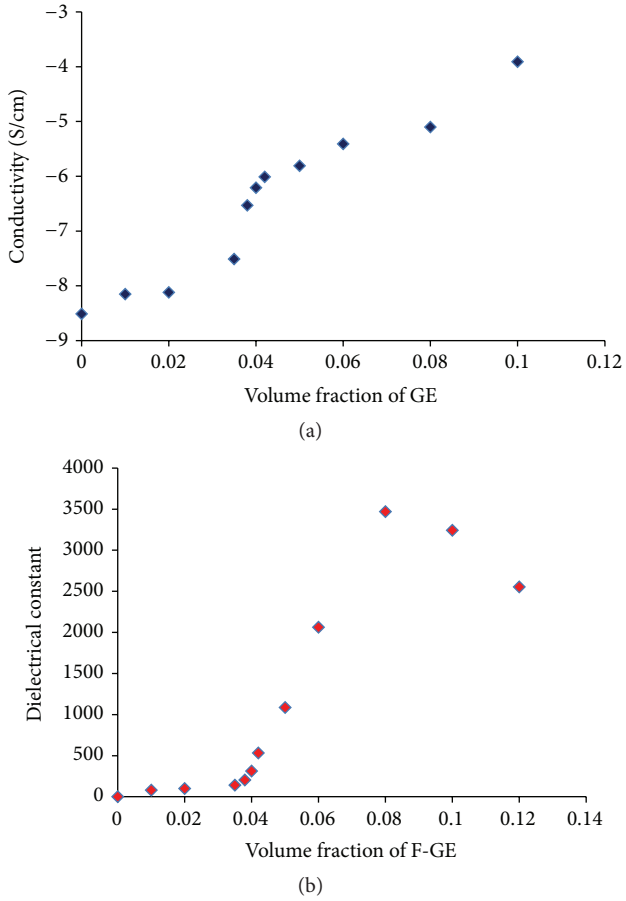

Figure 7: Dependence of (a) the electrical conductivity and (b) dielectric constant of GE-CH-PMNA composite on the volume fraction of F-GE.

threshold p_c increases slowly with increasing GE volume fraction. The reason for this can be attributed to the tunneling conduction mechanism and percolation phenomenon. The carboxylic groups on GE surface can reduce the tunneling current.

Figure 7(b) shows the change in dielectric constant of GE-CH-PMNA composite as a function of the volume fraction of F-GE. As seen in the figure, the dielectric constant increases rapidly when the volume fraction of F-GE increases from 4 to 8 vol%. Then, the dielectric constant is found to decrease with increase in F-GE concentration. The maximum value of dielectric constant of the GE-CH-PMNA composite is observed to be 3200 which is obtained at 8 vol% of F-GE at 1 kHz frequency. Dielectric properties were measured using an LCR meter (Agilent, E4980A) equipped with a dielectric test fixture (Agilent, 16451B) at the frequency 20 Hz to 2 MHz and at room temperature. Pure PMNA and its GE-CH-PMNA powders were pressed in the form of a disc pellet with a diameter of 25 mm by applying a pressure of 50 MPa in a hydraulic presser and the average thickness of the pellet was about 1.0 mm.

The dielectric properties of the composite have been explained by the percolation theory and interfacial polarization effect. In these composites, GE is distributed in the insulting matrix, which can form a lot of interfaces. When the concentration of GE increases, the number of interfaces also increases. This increases the dielectric constant with increasing GE concentration. When the concentration of GE is made larger than the percolation threshold of the composite, it results in agglomeration of GE. In this case, the interface between GE and CH will decrease, thus resulting in reduction in dielectric constant with further increase in GE concentration. Probably the π-orbital of the GE also creates large domains for nomadic electrons. These electrons can produce interfacial polarization effect. Moreover, the carboxylic groups present in functionalized GR are electron-withdrawing groups that will strengthen interfacial polarization. The large value of dielectric constant (3200 at 8 vol% of F-GE) observed for GE-CH-PMNA composite can be attributed to increasing number of interfaces formed by F-GE and CH matrix.

4. Conclusion

In summary, we have successfully fabricated GE-CH-PMNA as a new form of graphene-based nanocomposite and investigated its physical, chemical, and electrical properties with various compositions. Material characterizations performed using various measurements such as XRD patterns, SEM images, FTIR spectra, TGA, and DSC measurements indicate homogeneous dispersion of GE nanoplatelets within the CH-PMNA polymer matrix. The electrical conductivity and dielectric properties of the GE-CH-PMNA nanocomposite have also been investigated. Increase in conductivity and dielectric constants has been observed with increasing F-GE volume fraction. Due to the prominent electrical properties of PMNA and nanodimension of GE-CH-PMNA, such nanocomposites can find applications as cathode materials in batteries and electronic devices.

Competing Interests

The authors declare that they have no competing interests.

Acknowledgments

The authors acknowledge the support of characterization facility at CIPET, Bhubaneswar, India, for testing of their sample.

References

[1] C. N. R. Rao, A. K. Sood, K. S. Subrahmanyam, and A. Govindaraj, "Graphene: the new two-dimensional nanomaterial," *Angewandte Chemie—International Edition*, vol. 48, no. 42, pp. 7752–7777, 2009.

[2] K. S. Novoselov, V. I. Fal'Ko, L. Colombo, P. R. Gellert, M. G. Schwab, and K. Kim, "A roadmap for graphene," *Nature*, vol. 490, no. 7419, pp. 192–200, 2012.

[3] V. Georgakilas, M. Otyepka, A. B. Bourlinos et al., "Functionalization of graphene: covalent and non-covalent approaches, derivatives and applications," *Chemical Reviews*, vol. 112, no. 11, pp. 6156–6214, 2012.

[4] X. Huang, X. Qi, F. Boey, and H. Zhang, "Graphene-based composites," *Chemical Society Reviews*, vol. 41, no. 2, pp. 666–686, 2012.

[5] V. Singh, D. Joung, L. Zhai, S. Das, S. I. Khondaker, and S. Seal, "Graphene based materials: past, present and future," *Progress in Materials Science*, vol. 56, no. 8, pp. 1178–1271, 2011.

[6] Y. Shao, J. Wang, H. Wu, J. Liu, I. A. Aksay, and Y. Lin, "Graphene based electrochemical sensors and biosensors: a review," *Electroanalysis*, vol. 22, no. 10, pp. 1027–1036, 2010.

[7] Y. Zhu, S. Murali, W. Cai et al., "Graphene and graphene oxide: synthesis, properties, and applications," *Advanced Materials*, vol. 22, no. 35, pp. 3906–3924, 2010.

[8] C. Soldano, A. Mahmood, and E. Dujardin, "Production, properties and potential of graphene," *Carbon*, vol. 48, no. 8, pp. 2127–2150, 2010.

[9] H. S. Chen, T. N. Cong, W. Yang, C. Tan, Y. Li, and Y. Ding, "Progress in electrical energy storage system: a critical review," *Progress in Natural Science*, vol. 19, no. 3, pp. 291–312, 2009.

[10] G. A. Snook, P. Kao, and A. S. Best, "Conducting-polymer-based supercapacitor devices and electrodes," *Journal of Power Sources*, vol. 196, no. 1, pp. 1–12, 2011.

[11] T. Kuilla, S. Bhadra, D. Yao, N. H. Kim, S. Bose, and J. H. Lee, "Recent advances in graphene based polymer composites," *Progress in Polymer Science*, vol. 35, no. 11, pp. 1350–1375, 2010.

[12] S. H. Ryu and A. M. Shanmugharaj, "Influence of long-chain alkylamine-modified graphene oxide on the crystallization, mechanical and electrical properties of isotactic polypropylene nanocomposites," *Chemical Engineering Journal*, vol. 244, pp. 552–560, 2014.

[13] S. Stankovich, D. A. Dikin, G. H. B. Dommett et al., "Graphene-based composite materials," *Nature*, vol. 442, no. 7100, pp. 282–286, 2006.

[14] T. Ramanathan, A. A. Abdala, S. Stankovich et al., "Functionalized graphene sheets for polymer nanocomposites," *Nature Nanotechnology*, vol. 3, no. 6, pp. 327–331, 2008.

[15] Y. R. Lee, A. V. Raghu, H. M. Jeong, and B. K. Kim, "Properties of waterborne polyurethane/functionalized graphene sheet nanocomposites prepared by an in situ method," *Macromolecular Chemistry and Physics*, vol. 210, no. 15, pp. 1247–1254, 2009.

[16] Y. Xu, Y. Wang, J. Liang et al., "A hybrid material of graphene and poly (3,4-ethyldioxythiophene) with high conductivity, flexibility, and transparency," *Nano Research*, vol. 2, no. 4, pp. 343–348, 2009.

[17] H. Quan, B.-Q. Zhang, Q. Zhao, R. K. K. Yuen, and R. K. Y. Li, "Facile preparation and thermal degradation studies of graphite nanoplatelets (GNPs) filled thermoplastic polyurethane (TPU) nanocomposites," *Composites Part A: Applied Science and Manufacturing*, vol. 40, no. 9, pp. 1506–1513, 2009.

[18] G. Eda and M. Chhowalla, "Graphene-based composite thin films for electronics," *Nano Letters*, vol. 9, no. 2, pp. 814–818, 2009.

[19] C.-P. Tien and H. Teng, "Polymer/graphite oxide composites as high-performance materials for electric double layer capacitors," *Journal of Power Sources*, vol. 195, no. 8, pp. 2414–2418, 2010.

[20] Z. Terzopoulou, G. Z. Kyzas, and D. N. Bikiaris, "Recent advances in nanocomposite materials of graphene derivatives with polysaccharides," *Materials*, vol. 8, no. 2, pp. 652–683, 2015.

[21] H. A. Becerril, J. Mao, Z. Liu, R. M. Stoltenberg, Z. Bao, and Y. Chen, "Evaluation of solution-processed reduced graphene oxide films as transparent conductors," *ACS Nano*, vol. 2, no. 3, pp. 463–470, 2008.

[22] D. A. Dikin, S. Stankovich, E. J. Zimney et al., "Preparation and characterization of graphene oxide paper," *Nature*, vol. 448, no. 7152, pp. 457–460, 2007.

[23] J. L. Vickery, A. J. Patil, and S. Mann, "Fabrication of graphene-polymer nanocomposites with higher-order three-dimensional architectures," *Advanced Materials*, vol. 21, no. 21, pp. 2180–2184, 2009.

[24] M. J. McAllister, J.-L. Li, D. H. Adamson et al., "Single sheet functionalized graphene by oxidation and thermal expansion of graphite," *Chemistry of Materials*, vol. 19, no. 18, pp. 4396–4404, 2007.

[25] A. B. Bourlinos, D. Gournis, D. Petridis, T. Szabó, A. Szeri, and I. Dékány, "Graphite oxide: chemical reduction to graphite and surface modification with primary aliphatic amines and amino acids," *Langmuir*, vol. 19, no. 15, pp. 6050–6055, 2003.

[26] S. Stankovich, D. A. Dikin, R. D. Piner et al., "Synthesis of graphene-based nanosheets via chemical reduction of exfoliated graphite oxide," *Carbon*, vol. 45, no. 7, pp. 1558–1565, 2007.

[27] R. Justin and B. Chen, "Characterisation and drug release performance of biodegradable chitosan-graphene oxide nanocomposites," *Carbohydrate Polymers*, vol. 103, no. 1, pp. 70–80, 2014.

[28] J. R. Potts, D. R. Dreyer, C. W. Bielawski, and R. S. Ruoff, "Graphene-based polymer nanocomposites," *Polymer*, vol. 52, no. 1, pp. 5–25, 2011.

[29] S. J. An, Y. Zhu, S. H. Lee et al., "Thin film fabrication and simultaneous anodic reduction of deposited graphene oxide platelets by electrophoretic deposition," *Journal of Physical Chemistry Letters*, vol. 1, no. 8, pp. 1259–1263, 2010.

[30] F. Ordikhani, E. Tamjid, and A. Simchi, "Characterization and antibacterial performance of electrodeposited chitosan-vancomycin composite coatings for prevention of implant-associated infections," *Materials Science and Engineering C*, vol. 41, pp. 240–248, 2014.

[31] D. Han, L. Yan, W. Chen, and W. Li, "Preparation of chitosan/graphene oxide composite film with enhanced mechanical strength in the wet state," *Carbohydrate Polymers*, vol. 83, no. 2, pp. 653–658, 2011.

[32] X. Wang, H. Bai, Z. Yao, A. Liu, and G. Shi, "Electrically conductive and mechanically strong biomimetic chitosan/reduced graphene oxide composite films," *Journal of Materials Chemistry*, vol. 20, no. 41, pp. 9032–9036, 2010.

[33] H. Yin, Q. Ma, Y. Zhou, S. Ai, and L. Zhu, "Electrochemical behavior and voltammetric determination of 4-aminophenol based on graphene-chitosan composite film modified glassy carbon electrode," *Electrochimica Acta*, vol. 55, no. 23, pp. 7102–7108, 2010.

[34] L. He, H. Wang, G. Xia, J. Sun, and R. Song, "Chitosan/graphene oxide nanocomposite films with enhanced interfacial interaction and their electrochemical applications," *Applied Surface Science*, vol. 314, pp. 510–515, 2014.

[35] M. R. Mohammadi, F. Ordikhani, D. J. Fray, and F. Khomamizadeh, "Template-based growth of titanium dioxide nanorods by a particulate sol-electrophoretic deposition process," *Particuology*, vol. 9, no. 2, pp. 161–169, 2011.

[36] M. Fang, J. Long, W. Zhao, L. Wang, and G. Chen, "pH-responsive chitosan-mediated graphene dispersions," *Langmuir*, vol. 26, no. 22, pp. 16771–16774, 2010.

[37] Y. Wan, Z. Lin, D. Zhang, Y. Wang, and B. Hou, "Impedimetric immunosensor doped with reduced graphene sheets fabricated by controllable electrodeposition for the non-labelled detection of bacteria," *Biosensors and Bioelectronics*, vol. 26, no. 5, pp. 1959–1964, 2011.

[38] M. K. Pati, P. Pattojoshi, and G. S. Roy, "Fabrication and characterization of graphene based nanocomposite for electrical properties," *Advances in Materials Physics and Chemistry*, vol. 5, no. 1, pp. 22–30, 2015.

[39] R. Devi, S. Relhan, and C. S. Pundir, "Construction of a chitosan/polyaniline/graphene oxide nanoparticles/polypyrrole/Au electrode for amperometric determination of urinary/plasma oxalate," *Sensors and Actuators B: Chemical*, vol. 186, pp. 17–26, 2013.

[40] X. Li, H. Zhou, W. Wu, S. Wei, Y. Xu, and Y. Kuang, "Studies of heavy metal ion adsorption on Chitosan/Sulfydryl-functionalized graphene oxide composites," *Journal of Colloid and Interface Science*, vol. 448, pp. 389–397, 2015.

[41] R. K. Layek, S. Samanta, and A. K. Nandi, "Graphene sulphonic acid/chitosan nano biocomposites with tunable mechanical and conductivity properties," *Polymer*, vol. 53, no. 11, pp. 2265–2273, 2012.

[42] J. Jagiello, J. Judek, M. Zdrojek, M. Aksienionek, and L. Lipinska, "Production of graphene composite by direct graphite exfoliation with chitosan," *Materials Chemistry and Physics*, vol. 148, no. 3, pp. 507–511, 2014.